Third International Conference on CFD in the Minerals and Process Industries
CSIRO, Melbourne, Australia
10-12 December 2003

DISCRETE PARTICLE SIMULATION OF GAS-SOLID FLOW IN A BLAST FURNACE

Z.Y. ZHOU[1], D. PINSON[1], H.P. ZHU[1], A.B. YU[1], B. WRIGHT[2] and P. ZULLI[2]

[1] Centre for Simulation and Modelling of Particulate Systems
School of Materials Science and Engineering
The University of New South Wales
Sydney, NSW 2052, Australia

[2] BHP Steel Research Laboratories
P.O. Box 202, Port Kembla
NSW 2505, Australia

ABSTRACT

Experimental observations revealed that the stagnant zone, which forms in the lower central part of a blast furnace, is an important feature of solid flow, and that it is affected strongly by gas flow. However, it is difficult to model this feature within the framework of continuum mechanics without empirical or arbitrary treatments. This paper reports the use of discrete particle simulation for solid phase, combined with computational fluid dynamics for gas phase, to examine the gas-solid flow behaviour. It is shown that the proposed approach can generate a stagnant zone at the lower part of blast furnace, consistent with experimental observations. The effects of gas flowrate, particle and wall properties are examined in terms of solid flow patterns, velocity field, and normal force structure.
KEYWORDS: gas-solid flow; discrete particle simulation; CFD; blast furnace; stagnant zone

NOMENCLATURE

C_{d0} fluid drag coefficient on an isolated particle
d particle diameter, m
$\mathbf{F}$ volumetric fluid-particle interaction force, $N \cdot m^{-3}$
$\mathbf{F}_{f0}$ fluid drag force on an isolated particle, N
$\mathbf{g}$ gravitational acceleration, $m \cdot s^{-2}$
I moment of inertia of particle, $kg \cdot m^2$
k_c number of particles in a computational cell
k_i number of particles in contact with particle i
$\mathbf{M}$ torque, N·m
m mass of particle, kg
p pressure, Pa
$\mathbf{R}$ vector from the mass centre of the particle to the contact point, m
Re Reynolds number
t time, s
$\mathbf{u}$ fluid velocity, $m \cdot s^{-1}$
$\mathbf{v}$ particle translational velocity, $m \cdot s^{-1}$
V volume of particle, m^3
ΔV volume of a computational cell, m^3

Greek

χ empirical coefficient defined by eq.(9)
ε porosity
μ viscosity, $kg \cdot m^{-1} \cdot s^{-1}$
ρ density, $kg \cdot m^{-3}$
$\boldsymbol{\tau}$ stress tensor, Pa
$\boldsymbol{\omega}$ particle angular velocity, s^{-1}
$\hat{\boldsymbol{\omega}}$ unit vector defind by $\hat{\boldsymbol{\omega}} = \boldsymbol{\omega} / |\boldsymbol{\omega}|$

Subscripts

c contact
d damping
f fluid
i particle *i*
ij between particles *i* and *j*
j particle *j*
n normal component
r rolling friction
t tangential component

INTRODUCTION

Blast furnace (BF) ironmaking is an important technology by which iron is efficiently reduced from iron-bearing particles. This is a very complicated chemical process in which the layered coke and ore particles descend from the furnace top due to gravity. During descent, the ore is reduced, becoming liquid (slag and iron) in the cohesive zone, then flowing down to the hearth, and the coke flowing toward the raceway. In the meantime, a high velocity air blast enters the furnace raceway and combusts coke to generate reducing gases and smelting energy for the process. Then those gases rise through the particle bed and escape from the top. Previous experimental studies showed that the stagnant zone (commonly called the "deadman"), which forms in the lower central part of blast furnace, is an important feature of the particle bed, and is strongly affected by gas flow and particle properties (Khodak and Borosov, 1970; Ichida *et al.*, 1991, Takahashi *et al.*, 1993; Takahashi *et al.*, 1996; Wright, 2001a). Several continuum mechanics models have been proposed to study the gas-solid flow at the macroscopic level within the blast furnace (Yagi, 1993; Chen *et al.*, 1993; Austin *et al.*, 1997; Zhang *et al.*, 1998; Zaimi *et al.*, 2000). But empirical or arbitrary treatments have to be employed in the continuum description of solid flow in order to predict the profile of the stagnant zone.

In recent years, discrete approach, based on the discrete element method (Cundall and Strack, 1979), has been applied to particle systems in many fields including process engineering, mining, and geophysics. It has been applied to various problems. The main difficulty in applying the discrete method lies in simulating real granular materials where a very large number of particles with various shapes are assembled. However, the approach still enables us to investigate the micromechanics of

Copyright © 2003 CSIRO Australia

granular materials in a way that can not be achieved by continuum approaches or experiments.

Wright (2001b) applied the discrete approach to the solid flow in a blast furnace and showed the approach is able to capture the important solid flow features. However, the effect of gas flow was not considered. In this work, a combined discrete particle simulation (DPS) and computational fluid dynamics (CFD) solution is applied. This approach has been successfully used at UNSW in the simulation of gas fluidization (Xu and Yu, 1997; Yu and Xu, 2003) and raceway phenomena (Xu *et al.*, 2000). This paper extends that approach to investigate the gas-solid flow in a blast furnace . The results are analyzed in terms of solid flow patterns, flow field, and force structure.

MODEL DESCRIPTION

Discrete particle simulation

A particle in a granular dynamic system undergoes translational and rotational motions as described by Newton's second law of motion. The governing equations for particle *i* can be written as:

$$m_i \frac{d\mathbf{v}_i}{dt} = \mathbf{F}_{f,i} + \sum_{j=1}^{k_i} (\mathbf{F}_{c,ij} + \mathbf{F}_{d,ij}) + m_i \mathbf{g} \quad (1)$$

$$I_i \frac{d\boldsymbol{\omega}_i}{dt} = \sum_{j=1}^{k_i} (\mathbf{M}_{t,ij} + \mathbf{M}_{n,ij}) \quad (2)$$

where $\mathbf{v}_i$, $\boldsymbol{\omega}_i$ are, respectively, the translational and angular velocities of particle *i.* The forces involved are: particle-fluid interaction force, $\mathbf{F}_{f,i}$, the gravitational force, $m_i\mathbf{g}$, and inter-particle forces between particles *i* and *j*, which include elastic force, $\mathbf{F}_{c,ij}$, and viscous damping force, $\mathbf{F}_{d,ij}$. The torque acting on particle *i* by particle *j* includes two components. One arises from tangential force, given by $\mathbf{M}_{t,ij} = \mathbf{R}_{ij} \times (\mathbf{F}_{ct,ij} + \mathbf{F}_{dt,ij})$, where $\mathbf{R}_{ij}$ is a vector from the mass centre of the particle to the contact point; and another one is the rolling friction torque given by $\mathbf{M}_{n,ij} = -\mu_{r,ij} |\mathbf{F}_{n,ij}| \hat{\boldsymbol{\omega}}_{n,ij}$, which slows down the relative rotations of particles. For a particle undergoing multiple interactions, the individual interaction forces and torques are summed for the k_i particles interacting with particle *i*. The inter-particle forces are calculated based on non-linear models which can be found elsewhere (Zhou *et al.*, 1999).

Governing equations for fluid phase

The continuum fluid field is calculated from the continuity and Navier-Stokes equations based on the local mean variables over a computational cell, which are written as:

$$\frac{\partial \varepsilon}{\partial t} + \nabla \cdot (\varepsilon \mathbf{u}) = 0 \quad (3)$$

$$\frac{\partial (\rho_f \varepsilon \mathbf{u})}{dt} + \nabla \cdot (\rho_f \varepsilon \mathbf{u}\mathbf{u}) = -\nabla p - \mathbf{F} + \nabla \cdot \varepsilon \boldsymbol{\tau} + \rho_f \varepsilon \mathbf{g} \quad (4)$$

where $\mathbf{u}$, ρ_f, p and $\mathbf{F}$ are the fluid velocity, density, pressure and volumetric fluid-particle interaction force, respectively; $\boldsymbol{\tau}$ and ε are the fluid viscous stress tensor and porosity which are given as:

$$\boldsymbol{\tau} = \mu_f \left[(\nabla \mathbf{u}) + (\nabla \mathbf{u})^{-1} \right] \quad (5)$$

$$\varepsilon = 1 - \sum_{i=1}^{k_c} V_i / \Delta V \quad (6)$$

where V_i is the volume of particle *i*, and k_c is the number of particles in the computational cell.

Calculation of fluid drag force

Di Felice (1994) proposed a correlation for the drag force on a particle of diameter *d* in a multi-particle system which covers a wide range of flow regimes and porosity. His equation, when applied to the DPS modelling, is written as (Xu *et al.*, 2000):

$$\mathbf{F}_{f,i} = \mathbf{F}_{f0,i} \varepsilon_i^{-(\chi+1)} \quad (7)$$

where ε_i is the porosity around particle *i*, taken as the porosity in the computational cell in which particle *i* is located. The fluid drag force on particle *i* in the absence of other particles, $\mathbf{F}_{f0,i}$, and the coefficient, χ, are , given by:

$$\mathbf{F}_{f0,i} = 0.125 C_{d0,i} \rho_f \pi d_i^2 \varepsilon_i^2 |\mathbf{u}_i - \mathbf{v}_i| (\mathbf{u}_i - \mathbf{v}_i) \quad (8)$$

and

$$\chi = 3.7 - 0.65 \exp\left[-(1.5 - \log_{10} \mathrm{Re}_i)^2 / 2 \right] \quad (9)$$

where $C_{d0,i}$, the fluid drag coefficient, and the particle Reynolds number, Re_i, are given as:

$$C_{d0,i} = (0.63 + 4.8 / \mathrm{Re}_i^{0.5})^2 \quad (10)$$

and

$$\mathrm{Re}_i = \rho_f d_i \varepsilon_i |\mathbf{u}_i - \mathbf{v}_i| / \mu_f \quad (11)$$

As the fluid drag force is known for each particle, the volumetric fluid-particle interaction force in a computational cell can be determined by:

$$\mathbf{F} = \sum_{i=1}^{k_c} \mathbf{F}_{f,i} / \Delta V \quad (12)$$

This definition reflects the principle of Newton's third law of motion. That is, the fluid drag force acting on individual particles reacts on the fluid phase from the particles in a computational cell.

Computational methodology

The computational methodology has been well documented elsewhere (Xu and Yu, 1997; Xu *et al.*, 2001), and hence only briefly described here. For discrete particle simulations, explicit time integration is used to solve the translational and rotational motions of the particles (Cundall and Strack, 1979). The conventional SIMPLE method is used to solve the equations for the fluid phase in the continuum model (Patankar, 1980). The combination of DPS and CFD is numerically achieved as follows. At each time step, the DPS will give information such as the positions and velocities of individual particles. From these, the porosity and volumetric fluid-particle interaction force in each computational cell are calculated. CFD will then use the information to determine the gas flow field, from which the fluid drag forces acting on the individual particles are calculated. Incorporation of the resulting forces into the DPS will produce information about the motion of the individual particles for the next time step. In this way, the CFD and DPS models are coupled via the fluid drag forces on the particles and satisfying Newton's third law of motion.

Simulation conditions

The geometry of the blast furnace used in this work is shown in **Figure 1a** with 4 particle diameter thickness. The simulation is started with the random generation of 14,000 uniform spheres without overlaps, followed by a gravitational settling process for 3 seconds. To simulate the combustion process, particles are removed at a certain rate (i.e. 2 particles every 100 time steps) from the raceway region and added back on top of the bed. Once the discharge begins, the number of initially packed

particles is recorded until no obvious change is observed. This state is regarded as steady state and calculation is terminated. The variables considered in this work are gas flowrate, particle and wall properties and cohesive zone shape. Different coloured particles are used to distinguish layers within the packed bed and act as time-lines. Each layer has the same number of particles and all particles in the simulation have the same properties. **Table 1** lists the particle and wall properties used. Gas density is 1.205kg·m^{-3}, and its viscosity is 1.8×10^{-5}kg·m^{-1}·s^{-1}. The computational grid for the CFD solution is 17×41 body fitted cells (**Figure 1b**).

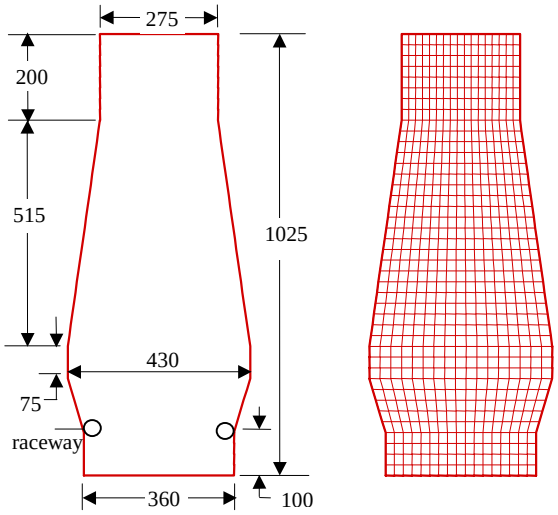

Figure 1: (a) Geometry of the blast furnace model used in discrete particle simulation (unit: mm); (b) computational grid for CFD solution

Table 1 Material properties used in simulation

Variables	Value
Particle shape	Spherical
Number of particles	14,000
Particle diameter	0.01m
Particle density	2500kg·m^{-3}
Sliding friction coefficient	0.4
Rolling friction coefficient	0.01*d*
Young's modulus	2.0×10^{6}kg·m^{-1}·s^{-1}
Possion's ratio	0.3
Time step	3.2×10^{-5}s
Simulation time	70s

RESULTS AND DISCUSSION

Model validity

The proposed model consists of two submodels: CFD for gas phase and DPS for solid phase. CFD modelling of gas flow, coupled with solid flow, has been well established (Chen *et al.*, 1993; Zhang *et al.*, 1998). Moreover, CFD-DPS modelling of gas-solid flow has been proved to be valid by the good agreement between the computed and measured results for gas-solid flow in the raceway (Xu *et al.*, 2001). Therefore, the present work of assessing the applicability of the proposed model is only focused on the

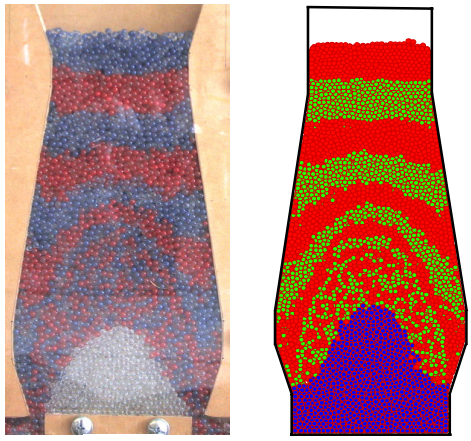

Figure 2: Comparison of solid flow patterns (a) experiment; and (b) simulation without gas flow

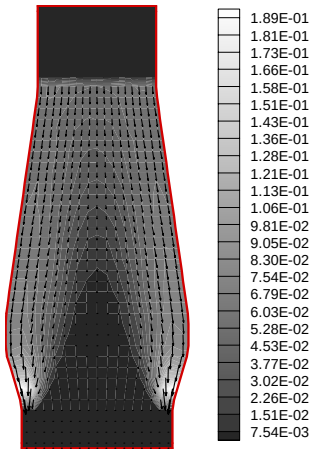

Figure 3: Time-averaged solid velocity field

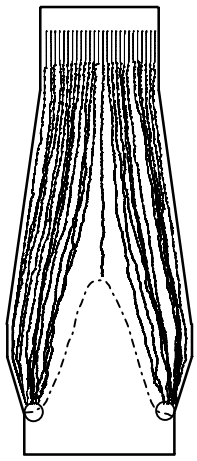

Figure 4: Trajectories of typical 26 particles (at the top from left to right, numbered 1~26)

DPS simulation which involves the change of geometry and material properties. For simplicity, it is conducted under the condition of no gas flow. In the DPS, the bed thickness is four particle diameters, and front and rear wall

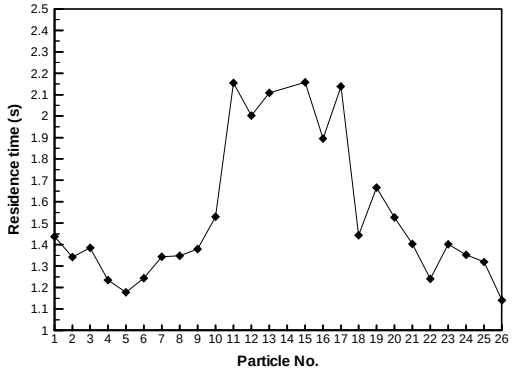

Figure 5: Residence time of the selected 26 particles

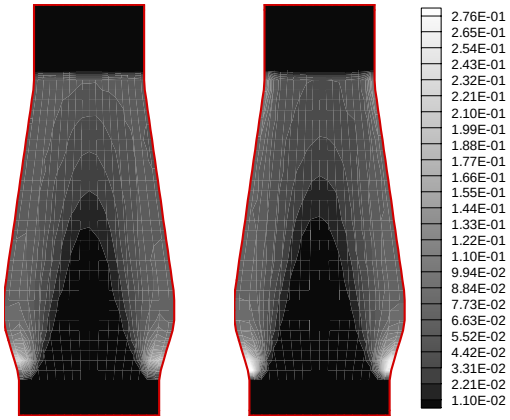

(a) (b)

Figure 6: Time-averaged solid velocity field for different gas velocity: (a) 6m·s^{-1}; (b) 15m·s^{-1}

boundary conditions are applied to match the experimental conditions. **Figure 2** shows the comparison of solid flow patterns observed in the experiment and simulation at steady state. The solid flow patterns and stagnant zone profiles are quite comparable in size and shape. **Figure 3** shows the time-averaged solid velocity field. It indicates that the motion of particles can be characterized by four regions: (1) plug flow in the upper part; (2) main funnel flow region through which the majority of the particles flow smoothly into the raceway; (3) stagnant region in the central bottom part where particles are almost motionless, and (4) quasi-stagnant region, bounded by the stagnant zone and the main flow region, where particles move slowly compared to the funnel flow region.

In order to observe the individual particle descent behaviour in the blast furnace shaft, 26 particles are initially placed across the top of the packed bed. Their trajectories are then traced and their residence times calculated. **Figure 4** shows the trajectories of those particles, indicating that most of the particles flow toward the raceway. However, particles at different positions have different trajectories. Particles adjacent to the central part move through the quasi-stagnant zone and experience longer residence times when compared to those far from the center (**Figure 5**).

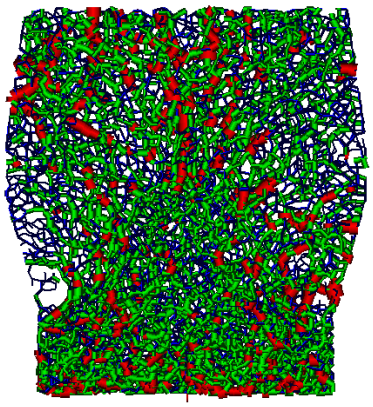

(a)

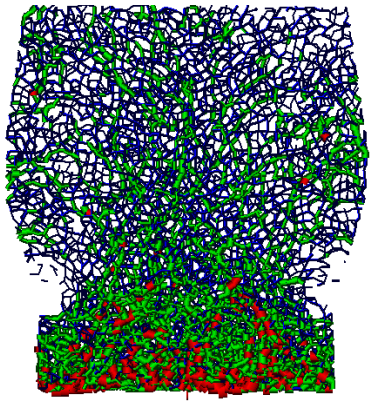

(b)

Figure 7: The network of normal forces between particles for different gas velocity: (a) 6 m·s^{-1}; (b) 15m·s^{-1}

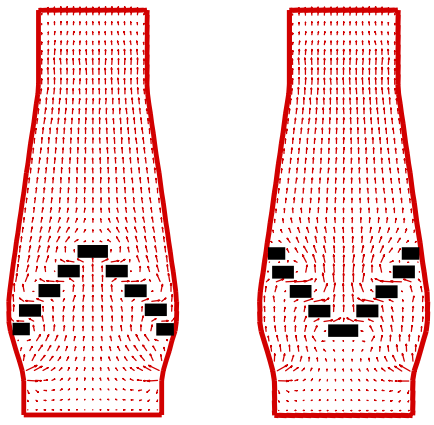

(a) (b)

Figure 8: Gas velocity vectors under the condition of (a) inversed V-shaped cohesive zone; and (b) V-shaped cohesive zone

All these observations are consistent with those in the literature (Takahashi *et al.*, 1993; Takahashi *et al.*, 1996; Zhang *et al.*, 1998; Wright, 2001a) confirming the applicability of the proposed approach.

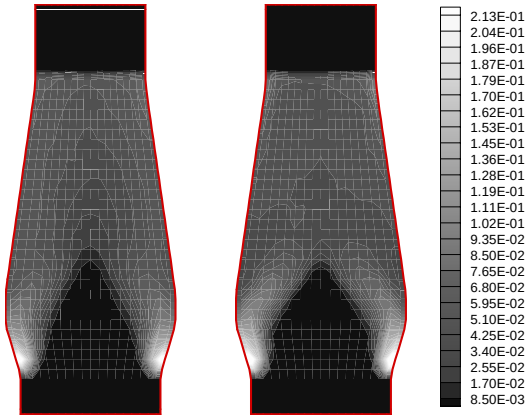

(a) (b)

Figure 9: Solid velocity field in slot model with inverse V-shaped CZ for different gas velocity: (a) 13m·s^{-1}; (b) 15m·s^{-1}

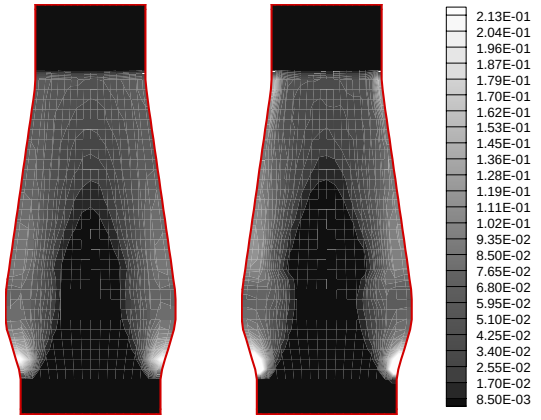

(a) (b)

Figure 10: Solid velocity field in slot model with V-shaped CZ for different gas velocity: (a) 13m·s^{-1}; (b) 15m·s^{-1}

Effect of gas flow

In blast furnace operations, the gas phase plays an important role in combusting coke to generate reducing gas and initiating the motion of particles. **Figure 6** shows the effect of gas flow on the time-averaged solid velocity field. It can be seen that particles in the raceway obtain higher velocities with increasing gas flowrate and the size of stagnant zone also increases with increasing gas flowrate. The results are quantitatively consistent with experimental observations (Wright, 2001a).

Inter-particle forces acting on individual particles in the low part of furnace are also examined. **Figure 7** shows the normal force network in the lower part of the furnace for different gas flowrates, where each stick represents one connection between two particle centres and its diameter represents the magnitude of the force. It is found that particle contacts become weaker as the gas flowrate increases. This is because as the gas flow increases, so does the drag force acting on the particle bed; as the proportion of the particles weight supported by the gas drag increases, the structure of particle bed becomes looser. The figures also revealed that particles in the stagnant zone experience the highest inter-particle forces. This is because these particles are supporting the weight of particles above them. Particles at the converging flow zone and around the outlets experienced low inter-particle forces.

Effect of cohesive zone

In operating blast furnaces, the softening and melting of ore particles will result in the formation of the so-called 'Cohesive Zone' (CZ). The CZ significantly influences the gas flow distribution in the lower part of the furnace shaft, which in turn may affect the solid flow. In this study, the CZ is represented by blocks which are impermeable to the gas phase but do not hinder the particle movement. **Figure 8** shows the gas velocity vectors with two assumed CZ shapes. Both show that the existence of the cohesive zone significantly changes the gas flow direction which would influence the particle flow behaviour around this region. The inverse V-shaped cohesive zone made the gas flow towards the periphery while the V-shape toward furnace centre.

Figures 9 and **10** show the time-averaged solid velocity fields for the two cohesive zones in the 2D slot model at different gas flowrates. In the case of the inverse V-shaped CZ, it is found that the stagnant zone becomes 'fatter' due to the strong gas horizontal velocity towards the periphery. However, in the case of V-shaped CZ, the stagnant zone became 'thinner', and 'taller'. This behaviour is considered to be due to the strong flow of gas towards the center.

3.4 Effect of wall

Experimental studies have shown that the stagnant zone is very small in the case of three-dimensional experiments (Wright, 2001a). A 2D slot model can be made to behave more like a full 3D model by reducing the friction between particles and the front or rear walls to a negligible level. **Figure 11a** shows the solid flow pattern when the front and rear wall sliding friction is 0.1 (the properties of the other walls are unchanged). Compared with **Figure 2b**, the stagnant zone is significantly reduced in size. It is therefore believed that wall friction plays a dominant role

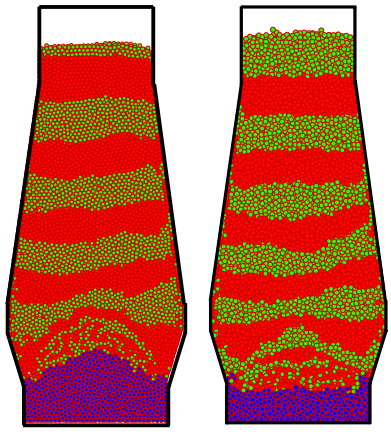

(a) (b)

Figure 11: Solid flow patterns (a) under the wall boundary conditions with particle-wall sliding friction coefficient is 0.1; and (b) periodic boundary conditions

in the formation of a large stagnant zone. To eliminate this effect, periodic boundary conditions are applied to the front and rear wall direction. As shown in **Figure 11b**, in this case, the stagnant zone becomes very small or even not identifiable which is consistent with the experimental observations (Wright, 2001a).

CONCLUSIONS

Discrete Particle Simulation (DPS), combined with Computational Fluid Dynamics (CFD), is used to investigate gas-solid flow in a 2D slot blast furnace model. The simulation results indicate that the approach is able to capture the characteristics of solid flow, and is in good agreement with experimental results. The flow patterns at the lower part of the furnace shaft is strongly affected by gas flow. Increasing the gas flowrate increases the size of the stagnant zone . There are strong force chains among the particles within the stagnant zone. The existence of a cohesive zone significantly influences the gas distribution, and hence solid flow behaviour. The size of stagnant zone is sensitive to the friction between particles and front/rear wall. When this interaction is low or periodic boundary conditions are used, the stagnant zone size is reduced which is consistent with experimental studies in the literature.

ACKNOWLEDGMENTS

The authors are grateful to BHP Steel Research Laboratories and Australian Research Council for the financial support of this work.

REFERENCES

AUSTIN, P.R., NOGAMI, H. and YAGI, J.I., (1997), "A mathematical model of four phase motion and heat transfer in the blast furnace", *ISIJ Int.*, **37**, 458-467.

CHEN, J.Z., AKIYAMA, T., YAGI, J.I. and TAKAHASHI, H., (1993), "Modelling of solid flow in moving beds", *ISIJ Int.*, **33**, 664-671.

CUNDALL, P.A. and STRACK, O.D.L., (1979), "A discrete numerical model for granular assemblies", *Geotechnique*, **29**, 47-65.

DI FELICE, R., (1994), "The voidage function for fluid-particle interaction systems", *Int. J. Multiphase flow*, **20**, 153-159.

ICHIDA, M., NISHIHARA, K., TAMURA, K. and SUGATA, M., (1991), "Influence of inner wall profile on descending and melting behaviour of burden in blast furnace", *ISIJ Int.*, **31**, 515-523

KHODAK, L.Z. and BOROSOV, Y.I., (1970/71), "Velocity and pressure distributions of moving granular materials in a model of a shaft kiln", *Powder Technol.*, **4**, 187-194.

PATANKAR, S.V., (1980), "Numerical heat transfer and fluid flow", Hemisphere, New York

TAKAHASHI, H. and KOMATSU, N., (1993), "Cold model study on burden behaviour in the lower part of blast furnace", *ISIJ Int.*, **33**, 655-663.

TAKAHASHI, H., TANNO, M. and KATAYAMA, J., (1996), "Burden descending behaviour with renewal of deadman in a two dimensional cold model of blast furnace", *ISIJ Int.*, **36**, 1354-1359.

WRIGHT, B., (2001a), "Model studies of solid flow in a blast furnace", Ph.D. Thesis, University of New South Wales.

WRIGHT, B., PINSON, D., YU, A.B. and ZULLI, P., (2001b), "Discrete particle simulation of granular flow in a blast furnace", 6th World Congress of Chemical Engineering, Melbourne, Australia, 23-27 September 2001

XU, B.H. and YU, A.B., (1997), "Numerical simulation of the gas-solid flow in a fluidized bed by combining discrete particle method with computational fluid dynamics", *Chem. Eng. Sci.*, **52**, 2785-2809.

XU, B.H., YU, A.B., CHEW, S.J. and ZULLI, P., (2000), "Numerical simulation of the gas-solid flow in a bed with lateral gas blasting", *Powder Technol.*, **109**, 13-26

XU, B.H., FENG, Y.Q., YU, A.B., CHEW, S.J. and ZULLI, P., (2001), "A numerical and experimental study of the gas-solid flow in a fluid bed reactor", *Powder Handling & Processing*, **13**, 71-76.

YAGI, J.I., (1993), "Mathematical modelling of the flow of four fluids in a packed bed", *ISIJ Int.*, **33**, 619-639.

YU, A.B. and XU, B.H., (2003), "Particle-scale modelling of gas solid flow in fluidization", *J. Chem. Technol. Biotechnol.*, **78**, 111-121.

ZAIMI, S., AKIYAMA, T., GUILLOT, J.B. and YAGI, J.I., (2000), "Sophisticated multi-phase multi-flow modelling of the blast furnace", *ISIJ Int.*, **40**, 322-331.

ZHANG, S.J., YU, A.B., ZULLI, P., WRIGHT, B. and TUZUN, U., (1998), "Modelling of the solids flow in a blast furnace", *ISIJ Int.*, **38**, 1311-1319.

ZHOU, Y.C., WRIGHT, B., YANG, R.Y., XU, B.H. and YU, A.B., (1999), "Rolling friction in the dynamic simulation of sandpile formation", *Physica A*, **269**, 536-553.